Materials & Design 252 (2025) 113809

Contents lists available at ScienceDirect

Materials & Design

journal homepage: www.elsevier.com/locate/matdes

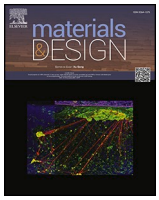

# 3D multi-site hydrogen evolution reaction catalysts on nanoimprinted surfaces, structured via multi-photon lithography derived masks

Alexander Jelinek [a,*], Daniela Neumüller [a,b], Christoph Gammer [b], Jürgen Eckert [a,b], Daniel Kiener [a]

[a] Department of Materials Science, Montanuniversität Leoben, Franz Josef-Straße 18, 8700 Leoben, Austria
[b] Erich Schmid Institute of Materials Science, Austrian Academy of Sciences, Jahnstraße 12, 8700 Leoben, Austria

ARTICLE INFO

*Keywords:*
Multi-photon lithography
Nanoimprint lithography
Physical vapor deposition
Hydrogen evolution reaction
Catalysis

ABSTRACT

Efficient water splitting is a major challenge in green hydrogen production and energy transition. Thus, considerable scientific efforts are devoted to optimize surface geometries for enhancing the performance of water-splitting catalysts. The current study aims to develop a reliable and facile 3-step (re-)production technique for manufacturing structured surfaces by combining multi-photon lithography (MPL) and nanoimprint lithography (NIL). MPL enables structuring of high-definition micrometer-scale surface geometries. A variation of these topologies was used as masks for replication by NIL. Thus, molds were derived to emboss the original nanostructured topologies repeatedly into a UV-curable resin. Subsequently, a Ni thin film metallization was deposited by physical vapor deposition onto the final imprinted polymeric structures, thereby realizing topologically structured conductive electrodes. To demonstrate the applicability of this elaborated technique, the catalytic activities towards the hydrogen evolution reaction were assessed for different surface geometries. An increase in catalytic performance was achieved through surface enlargement by structuring, whereby a direct contribution of the specific structure geometry was not evident. This elegant method is highly versatile and scalable for producing a wide range of structured functional surfaces on a lab scale, as demonstrated for the water splitting reaction, with results transferable to an industrial scale.

## 1. Introduction

The generation of green hydrogen from electric energy via electrolysis is an important topic of ongoing scientific research. To guarantee the economic compatibility of sustainably produced hydrogen, developing stable, non-noble metal catalysts for water-splitting reactions (hydrogen evolution reaction; HER, oxygen evolution reaction; OER) presents a major concern in energy transition [1]. In general, two strategies are applied in catalyst design, whereby the activity of a catalyst can be either tuned by increasing the intrinsic activity (chemical composition, alloying [2], intercalation, polymorphs, core–shell structures) or by increasing the number of active sites in the system (nanostructuring [3], nanoparticle loading and shape [4,5], substrate choice [6–8]). This also includes surface structuring as a successful measure to multiply the surface area [9] and implies a pure structural design related aspect. Ideally, both routes are combined to develop a suitable system capable of gradually displacing the gold standard noble metal catalysts in electrolysis. Many of these strategies, however, focus on small-scale material production and do not allow upscaling. Herein, we aim to develop a convenient and versatile method for fast large-scale production of catalyst materials, with the possibility to upscale to a technically relevant throughput, using Nanoimprint Lithography (NIL) and Multi-Photon Lithography (MPL).

NIL is a promising method to produce nanostructured surfaces on scalable areas by replicating a mold [10–13]. Up to now, many materials have been nanoimprinted through a variation of processes [12,14]. Herein, thermosets obtained through resin curing are used. A thin liquid film of resin is applied onto a substrate. Subsequently, a mold made from a flexible polymer [15] is pressed onto the film while the resin is cured simultaneously. Due to the direct contact between the resin and the mold, this technique is highly precise, while being limited solely by the curing rate of the resin. The principle can be realized via flat molds to emboss flat surfaces [11,16] or through a roll-on process [17–20] to achieve high throughput and cost efficiency [10].

* Corresponding author.
*E-mail address:* alexander.jelinek@unileoben.ac.at (A. Jelinek).

https://doi.org/10.1016/j.matdes.2025.113809
Received 17 January 2025; Received in revised form 24 February 2025; Accepted 4 March 2025
Available online 5 March 2025

MPL provides a versatile way of producing the described NIL masks. This technique employs a photocurable resin to manufacture the original structure required for imprinting. The used polymer system is cured by multi-photon polymerization. The process is triggered via multi-photon absorption by a photoinitiator leading as a consequence to activation and curing. MPL writing is characterized by its high resolution, precision and versatility regarding structures, thus is a production method suitable for individual needs, with only a few limitations such as the inability to deposit unsupported material [21].

The present work aims to investigate the potential of MPL-derived masks for the production of surface-structured electrodes. The combination of MPL and NIL techniques promises a flexible structural design with short iteration cycles (by MPL), and fast and reliable reproduction (by NIL). Additionally, the merge of techniques enables the use of a broad range of materials including non-transparent, highly filled, and even time-sensitive or thermally cured resins with retarded polymerization, which might be beneficial for future substrate material improvements.

In the present work, a process outlined in Fig. 1 was chosen. Firstly, various surface structures on the micrometer scale were produced through MPL and replicated by NIL. Subsequently, a metallization step was required to add a conductive and catalytically active film to the system to deliver fully operational electrodes for hydrogen evolution experiments. Therefore, pure Ni was employed as a well-known electrode material with good HER performance for non-noble metals [22]. Physical vapor deposition (PVD) as a comparably gentle and surface-preserving technique was selected to deposit a metallic Ni thin film on top of the NIL structures. Finally, the HER performance of these MLP-NIL-derived electrodes was assessed [2]. Different surface structures are compared to demonstrate the versatility of the process enabled by the utilization of MPL.

To the authors' best knowledge, there have been no reports of investigations concerning PVD thin film electrodes deposited onto NIL replicated structures produced from MPL-derived masks. Therefore, we focus on the aspects of surface structuring. Further, the use of the outlined process specifically for producing metalized HER electrodes is demonstrated. Finally, possible applications are assessed. Structure replication is considered the key aspect of this process since the high-resolution MPL manufacturing is time-consuming and therefore unsuitable for producing multiple electrode pre-structures. Initial surface design and preceding structure selection considerations are addressed and transparently discussed in the supplementary material. From this starting point, the repeatability of the replication process is assessed, reflected in the magnitude of scatter within the performance of the electrodes derived. Finally, the absolute effect of structural design choices, will be rated by exemplary application in regarding hydrogen evolution reaction catalysis and performance evaluation The aim is to give a holistic application-based assessment of the developed aspects and procedures. It should be emphasized here, that we introduce a scalable process for potentially accelerating the development and production of structured electrodes suitable for various applications.

## 2. Experimental

The initial structure design process started with the selection of different micrometer-sized surface structures (dome, cylinder, prismatic star). The selected surface structures were printed in a square grid-like manner spanning 500 × 500 $\mu m^2$ for each type. After successful mask writing, molds were cast and NIL replication was conducted with a commercial photoresist. The obtained replicas and a flat film as reference were subjected to a PVD coating process to apply a conductive Ni coating. Masking was used to ensure that all samples had identical geometric surface areas. Finally, hydrogen evolution experiments were conducted on the structured Ni thin film electrodes to assess their catalytic performance, as detailed below.

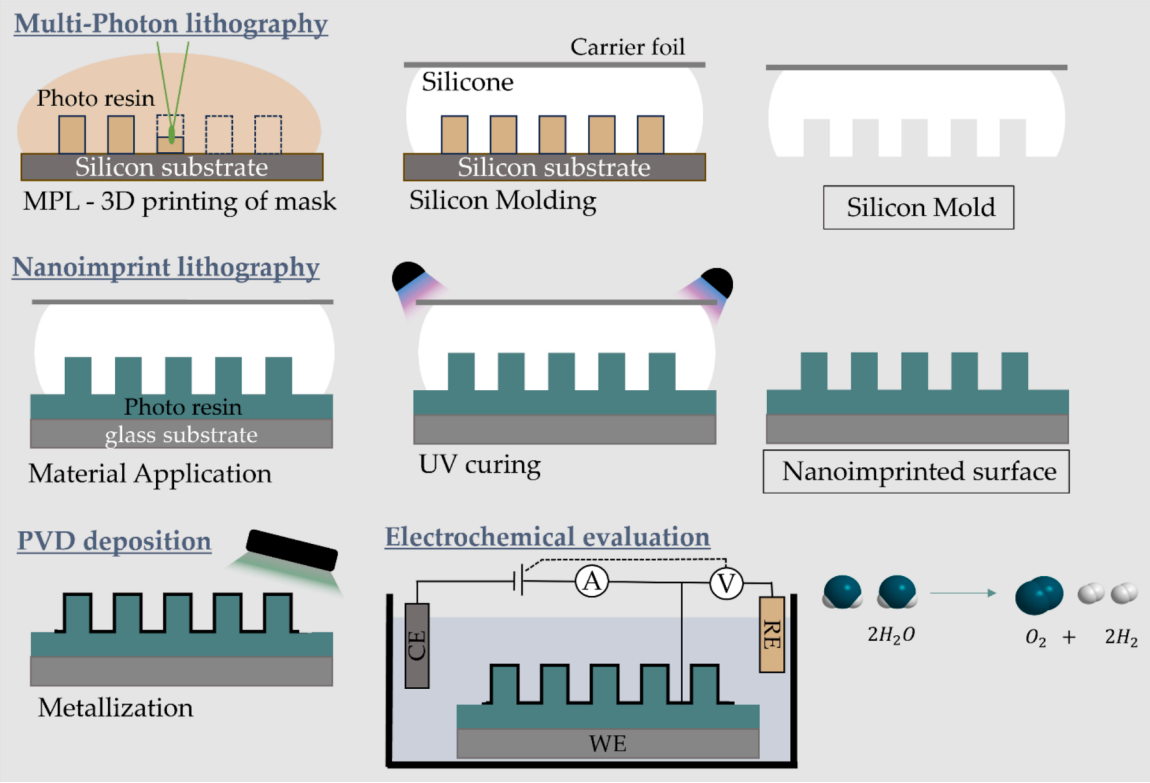


**Fig. 1.** Illustration of the process developed within this work. Starting from geometrically advanced MPL structures, NIL replication was performed and PVD sputtered films were subsequently deposited to serve as electrodes on the replica for final hydrogen evolution experiments. WE: Working electrode, CE: Counter electrode, RE: Reference electrode.

### 2.1. Surface structure design

To examine potential constraints of the replication process, various structures were subjected to a selection process during the initial structural investigation. Therefore, the process described in the following was applied to a single substrate containing various geometries (see supplementary **Fig. S1**). The results are displayed in detail in the supplementary section and also briefly addressed in the results section. From the preliminary investigated structures, dome, cylinder, and prismatic star shapes were selected due to the increasing length of exposed edges while preserving reliable NIL forming. Edges were considered as important geometrical characteristic since they are known to provide HER-catalytically active sites [23,24] and thus potentially influence the activity of certain structures.

The domes were designed with a diameter of 3.5 μm, and the cylinders with a diameter of 3 μm. The star-shaped prisms had a regular 5-fold star footprint with an outer diameter of 3 μm and an inner diameter of 1.5 μm, respectively. The surface area increase (compared to a flat surface) of the dome was used to scale the height of the other two geometries. All surface structures were constructed in a way to nominally increase the overall surface area by 60 % concerning the flat surface in theory. The geometric shapes were designed with CAD software (FreeCAD, version: 0.20). For further processing, a slicing software, included in the MPL device software package (DeScribe 2.7, Nanoscribe GmbH & Co. KG, Eggstein-Leopoldshafen, Germany) was used.

### 2.2. NIL mask writing via MPL

For model multiplication, each structure design was multiplied in the MPL software using the array function. The structures were arranged in two perpendicular axes 20 times in each direction with a defined spacing of 4 μm between the centers. A preview of the structural layout is illustrated in Fig. 2. Since the device covers only a limited field of view, consecutive stitching of smaller sections (single print job: $80 \times 80\ \mu m^2$) was necessary. This was implemented by consecutive shifts of the printer stage commanded through the MPL devices instruction language. Thus, a full print job was obtained, with a total area of $2.5 \times 2.5\ mm^2$. This resulted in 250 000 structures per mask, neglecting stitching artefacts such as slightly overlapping structures.

The NIL mask writing was carried out with a dedicated MPL device (Photonic Professional GT2, NanoScribe GmbH & Co. KG, Eggstein, Leopoldshafen, Germany) onto a pre-silanized silicon substrate. The silanization procedure was required to guarantee enhanced surface adhesion, specifically for the later molding process. The procedure stands out due to its simple design and is described in detail in a previous publication [21]. A 63x objective (Plan-Apochromat 63x N.A. 1.4 Oil DIC, Carl Zeiss AG, Oberkochen, Germany) with the dedicated proprietary photo resin IP-DIP (Nanoscribe GmbH & Co. KG, Eggstein-Leopoldshafen, Germany) was used. This combination is specified for the highest resolution on the employed platform. The standard processing parameters were reproduced (slicing distance 300 nm, hatching distance 200 nm). To obtain a more uniform final appearance and accommodate for the feature size, a 90° shift was introduced between consecutive printed layers.

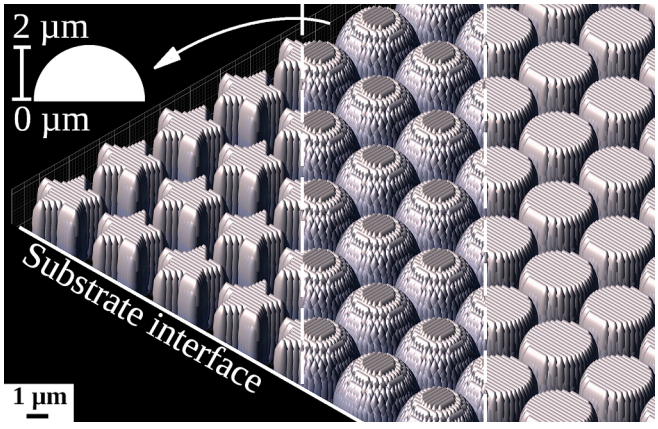


**Fig. 2.** Preview of the designed and arranged structures obtained via the MPL device software. The depicted surface structures (stars, domes and cylinders) were printed on individual substrates to act as NIL masks.

### 2.3. NIL PDMS molding

For deriving PDMS molds a standard two-component resin (Silixon10, Silikonfabrik.de, Bad Schartau, Germany) was used, specified for a feature size down to 1 μm. PDMS was selected regarding its low stiffness, facilitating the later peel-off without damaging the MPL-mask structures, nor the mold itself or the finally replicated ones. Therefore, the cavities are not clogged by mask remnants and multiple molds can be derived from one precursor structure.

The base component and the hardener of the PDMS resin were mixed with a 1:1 wt ratio. The mixture was homogenized and subsequently degassed in a vacuum desiccator, with multiple vacuum cycles until no further bubbles emerged. The PDMS resin (6–8 drops) was applied to the substrate, starting near the printed structures. By adding small portions of resin at a time the liquid slowly covered firstly the structured region and then a large portion of the mask area around. With this approach, no bubbles were trapped close to the structured region and a decently thick mold was formed. For the mold basis, a piece of well-adhering etched PP foil, with dimensions of around $3 \times 3\ cm^2$, was placed on top of the liquid resin without applying force to preserve the mask elements. By pure surface tension between film and MPL-substrate, the PDMS resin was drawn outwards to cover the entire area of the substrate. After curing for at least 24 h the mold was peeled, starting from one edge, whereby special attention was paid to avoid contact between mold and mask after separation.

### 2.4. NIL forming

A standard and easily available UV curable photo resin (translucent UV resin – clear, Anycubic Technology Co Ltd., Hongkong, China), originally designed for conventional direct laser processing printers, was chosen for the NIL process. Soda-lime glass slides were prepared with dimensions of roughly $25 \times 25\ mm^2$ to be used as NIL substrate. After scribing and splitting, the edges were rounded by sand paper to simplify handling.

For the actual replication process, 6–8 drops of bubble-free resin were directly applied onto the mold. Starting from an unstructured region and by adding further resin drop by drop, the structured region was slowly covered in a controlled way. Therefore, any bubble formation or trapping of air in the cavities was avoided. A substrate glass piece was put onto the resin without any additional force. For illumination, a 6 W 405 nm UV lamp (Sovol, Shenzhen, Guangdong, China) with an opening angle of 120° was employed for UV resin curing. The stack was illuminated for ~ 1 min with a distance of 20 cm to fully cure the photo resin. Due to the released heat, the stack was subsequently allowed to cool down for a few minutes before peeling the PDMS mold starting from one edge, where again contact between mold and imprint after separation was strictly avoided. To create a flat reference surface without any structures, a few drops of photoresist were cured between a substrate and a glass slide.

### 2.5. Preparation of electrode masks

For enhanced control over geometric electrode areas, self-adhering shadow masks were used to guide thin film deposition on the produced structured substrates. For this, two layers of galvanic tape (Circuit Plating Tape 1280, 3M, St. Paul, MN, USA) were cut by a commercial cut

plotter (Cricut Explore Air 2, Cricut, South Jordan, Utah, USA), with the shape defined in the corresponding software (Cricut Design Space v8.21.54), consisting of a $4 \times 4$ mm$^2$ square with a 3 mm wide contact bar, facilitating the later use as an electrode. The self-adhering shadow masks were applied on the prepared NIL imprinted specimens with the structured surface in the center of the square before sputter deposition. After removing the tape after metal coating, the process yielded structured electrodes with a defined surface area.

### 2.6. Thin film deposition

Metallization of the cured structures was done via magnetron sputter deposition using a small-scale sputtering device (HEX, Korvus Technology Ltd, High Wycombe, United Kingdom), equipped with a fission DC sputtering source. A Ni target with a 2 inch target diameter, a purity of 99.999 % (HMW Hauner GmbH & Co.KG, Röttenbach, Germany), and a thickness of 1 mm was used. The magnetic properties of Ni demand the use of a strong magnetron (available from Korvus Technology Ltd.) for deposition. Plasma ignition was done in power-controlled mode with an Ar flow of 100 sccm at an average pressure of $6.5 \times 10^{-3}$ mbar. The deposition power was set to 80 W for Ni deposition. The sample stage was rotated at 20 rpm and the Ar flow was set to 20 sccm, reaching an overall chamber pressure of $\sim 2 \times 10^{-3}$ mbar during the process. The deposition time was set to 30 min to reach an estimated film thickness of $\sim$ 300 nm. The film thickness was verified by Confocal Laser Scanning Microscopy (CLSM) imaging (LEXT OLS4000, Olympus Corp., Tokyo, Japan). The selected parameters are based on a previous work and achieve continuous thin films that provided complete coverage and low initial roughness [25]. Special care was taken to achieve reproducibility and comparability within this article regarding the results of thin film deposition.

### 2.7. Electrochemical measurements

Electrochemical measurements were conducted using a three-electrode setup combined with a potentiostat (PARSTAT4000A, Ametek Inc., Berwyn, PA, USA) including the VersaStudio software (version: 2.60.6). The measurements were conducted in 1 mol/l KOH (99.99 % purity; Sigma–Aldrich) electrolyte employing a high surface graphite rod as counter electrode and a Hg/HgO reference electrode (ALS Co. Ltd., Tokyo, Japan) for alkaline solutions as a reference. The structured and metalized working electrodes were prepared as described above.

To obtain HER polarization curves, cyclic voltammetry (CV) was employed to monitor the activities of the prepared catalysts in the range between −0.75 and 1.4 V vs. Hg/HgO at a scan speed of 50 mV/s. For data evaluation, the back loop of the third CV was analyzed. To guarantee reproducibility, each experiment was repeated at least three times. The potentials reported herein were converted to the reversible hydrogen electrode (RHE) potential.

### 2.8. Surface topography evaluation

Confocal laser scanning microscopy (CLSM) was employed to monitor the metalized 3D structures and to calculate the projected surface area for electrochemistry. Atomic force microscopy images were obtained using an atomic force miscrioscope (AFM) (Bruker Dimension Icon, Bruker Corp., Billerica, MA, USA) in tapping mode, equipped with an RTESPA-300 probe and corresponding software (NanoScope. Version: 10.0) for assessing surface characteristics. For data analysis and image visualization, the Gwyddion data analysis software was used [26]. The roughness factor ($R_F$) was calculated from the topography images. All scanning electron microscopy (SEM) images (AURIGA, Carl Zeiss AG, Oberkochen, Germany) were obtained with 5 kV acceleration voltage, an aperture size of 30 μm and a working distance of 11.5 mm.

## 3. Results

First, a variation of structures was produced via MPL and subsequently rated concerning NIL replicability and uniformity of the applied coatings. Based on this holistic structure screening the shapes used for structured electrode manufacturing presented in this work were chosen. The reviewed structures and models and the advantages and disadvantages of the explored range are summarized in the supplementary material **Fig. S2.** The homogeneity of PVD on the structures was analyzed by depositing a metallic thin film onto the structures presented in **Fig. S2**. The analysis of coating homogeneity revealed a visible effect of shadowing originating from the structural features and strongly influenced by their dimensions (see **Fig. S3**). Due to the line-of-sight coating characteristics of PVD, strongly inclined and shadowed regions exhibit considerably reduced film thickness. Significant deviations are particularly evident at the edges of structures on vertical surfaces. To achieve a uniform metal thin film on the chosen electrode structures, it was essential to maintain a height-to-diameter ratio of less than 1. A homogenous thin film thickness and coverage are crucial to avoid damage during periodic catalyst electrochemical testing. Applying the NIL process described above, a PDMS mold was produced, which was further used for the replication of the structures. The replicas were equally coated with a metallic thin film (see **Fig. S4**) to assess the final result of the combined processes. Thin, single-line structures could not be replicated, and high aspect ratio structures tended to be lost in the NIL process. The film thickness along the structure perimeter seems to be more uniform on replicated structures, presumable due to rounded edges. Thus, in addition to the decreased aspect ratio, the general size was increased by a factor of two for the selected structures. Within the PVD film pores developed, presumably due to the intrinsic roughness of the MPL process, which cannot be prevented. However, the pores seemed reduced on replicated structures, leading to a more uniform film appearance compared to coatings on the original structures. Ultimately this extensive structure investigation led to the selection of the following three shapes: cylinders, domes and star-shaped prisms (see Fig. 2). Those structures were further produced on a larger scale to be suitable as NIL masks for electrode surface structuring.

Ni thin film electrodes were produced as outlined in Fig. 1. Before evaluating the catalytic activities, the electrodes were structurally analyzed using various techniques. As a first analysis step, CLSM was used to check the thin film quality and get an overview of the electrode surfaces, depicted in Fig. 3**(a)**. The square-shaped surface-structured region (featuring domes, cylinders and stars) was easily distinguishable from the flat region at low magnification. A magnified section of the cylindric surface structures is depicted in Fig. 3**(b)**. The surrounding non-structured Ni surface was found to feature very low roughness and high reflectivity and thus brighter appearance in the microscope images. A corresponding AFM topography evaluation (see Fig. 3**(c))** confirmed the extraordinarily low roughness in the nanometer range of the non-structured electrode parts. Any features in this area originate from substrate manufacturing (molding, demolding, curing), sputter deposition, or enclosed impurities. Consequently, the surface area increase through roughness was close to zero, and it was thus assumed further that the geometric area is very close to the real surface area in this region. The Ni deposition parameters were developed elsewhere [25], focusing on structure and grain size as well as optimized adhesion to the substrate and film stresses while obtaining smooth thin films excluding roughness arising through the deposition process. Upon a detailed investigation of the electrode surfaces, hairline cracks were visible in several Ni thin films. It is assumed that the cracks occur due to different coefficients of thermal expansion and mechanical properties of the polymeric substrate base and thin film Ni causing film stress. Besides that, the Ni film exhibits qualitatively good adhesion on the polymeric substrate underlined by micro scratch tests conducted and (see **Fig. S5**) and described in the supplementary material in detail. In short, the film shows low delamination tendency, but chipping of the brittle polymeric

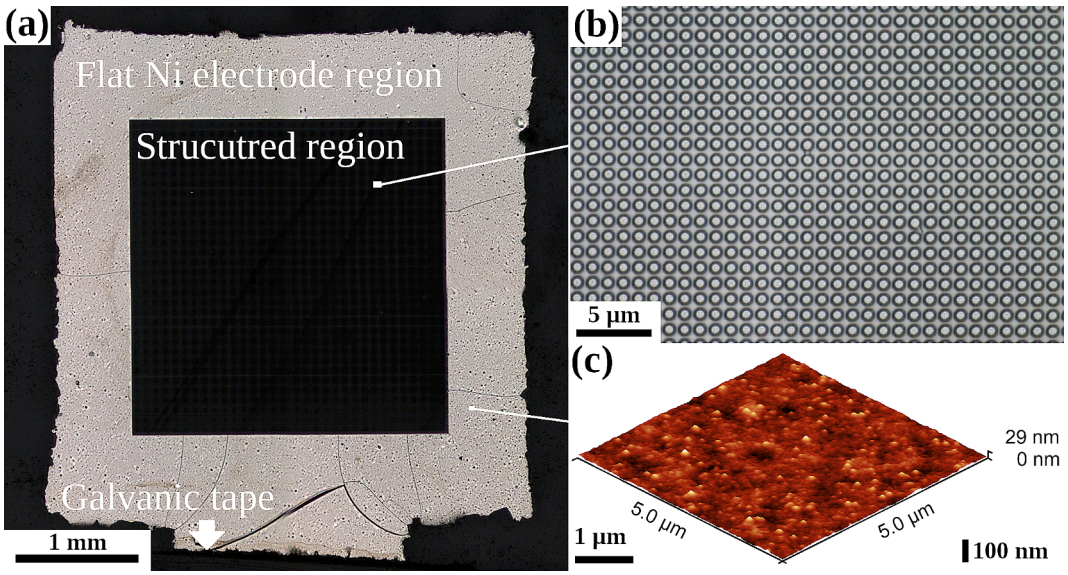


**Fig. 3.** Representative NIL structured Ni thin film electrode. (a) Overview CLSM image with functional sections marked. The electrical contact leads out towards the bottom, covered with tape for insulation and a defined surface area. (b) High magnification top-view image of the structured region, showcasing cylindrical features. (c) AFM height topography image of the flat, unstructured electrode surface, documenting surface roughness in the nanometer regime.

substrate was the predominant failure mechanism prohibiting a detailed analysis. However, possible consequences of poor film adhesion or stress and cracks will be discussed later. The obtained film thickness was evaluated through surface height profiles on a silicon reference specimen, half covered during deposition, yielding a thickness of 279 ± 5 nm.

For subsequent testing and evaluation, detailed information about the electrode geometry and surface characteristics was necessary. The total electrode areas (as depicted in Fig. 3**(a)**) were 15.70 ± 0.30 $mm^2$ (Standard deviation) with the structured part showing a surface area of 6.56 ± 0.17 $mm^2$. For the surface structures, the initial design goal for all structures was a roughness factor $R_F = \frac{A_{real}}{A_{geom}} = 1.6$, since the targeted surface increase was 60 % compared to the flat surface.

Selected SEM images of the individual structures are depicted in Fig. 4, showing details of well-replicated structures with a smooth Ni coating. The visible horizontal lines on all structures originate from stepwise MPL manufacturing. These details were further replicated along the NIL process and led to structural precursors during Ni film growth. Besides, the edges were smoothed, which is visible on the cylindric (Fig. 4**(a)**) and star-shaped structures (Fig. 4**(c)**), which even appeared reduced in size due to the loss of the star's vertical edges. In comparison, the dome structures (Fig. 4**(b)**) were extraordinarily well replicated and most resembled the original MPL layout.

In addition to the SEM investigations, CLSM height images were originally acquired as complementary analyses to determine the deviation from the ideal shape. From the height images, a 3D image can be constructed (see **Fig. S6**) and the surface area (enlarged due to structuring) can be calculated. However, due to arising edge artefacts in CLSM imaging, we decided against using the derived values for the calculated surface area. Instead, idealized values for the surface area increase ($R_f = 1.6$) were used. The CLSM image analysis, including obtained $R_F$ values, and data evaluation is included in the supplementary material. From a qualitative perspective, the effect of structuring on the surface area was confirmed, along with the perception of smaller surface areas for the star structures.

For the electrochemical measurements, the $R_F$ of the structures is not to be mistaken for the effective $R_{F,eff.}$ of the entire electrode. For $R_{F,eff.}$, the surface increase by the structured part was calculated for the overall electrode surface, thus also including the non-structured electrode part. The ideal $R_{F,eff}$ was calculated to be 1.25, taking into account the actual electrode proportions.

## 4. HER activity of structured thin film electrodes

Sputter-deposited and structured electrodes were further tested for their catalytic activity towards HER. In theory, two concepts can be taken advantage of in this regime. On one hand, catalyst efficiency is boosted by an increased surface area [9]. This does not alter the intrinsic catalytic properties of the material; however, it can reduce the necessary catalyst loading and contributes therefore to process optimization. On the other hand, kinks, terraces, and edges are known to provide catalytically active sites within the material [23,24]. By artificial modification and generation of such sites, one expects a positive influence on the catalytic process. Notably, both parameters are addressed with the

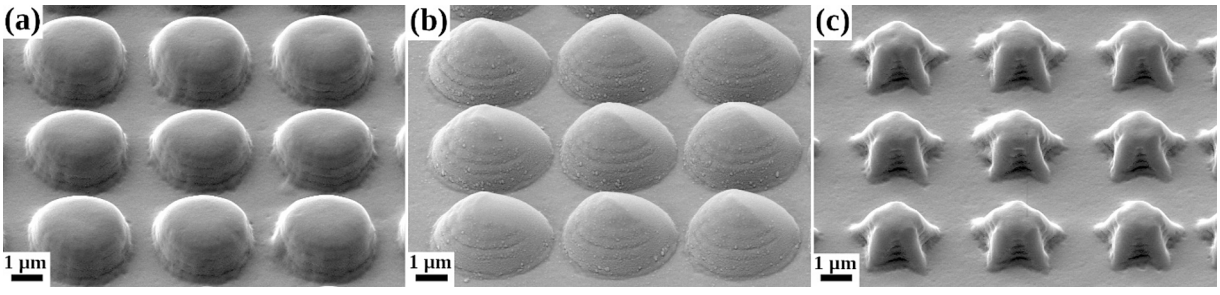


**Fig. 4.** Representative SEM images of the surface structures obtained after NIL replication and Ni coating.

outlined experimental design.

For evaluation of the structured electrodes, linear polarization curves were analyzed. The reported overpotentials ($\eta_{10}$) were evaluated at −10 mA/cm$^2$ [2], analyzing the back loop of the third recorded cycle. The resulting polarization curves are shown in Fig. 5**(a)**. The displayed data is given for the geometric area for comparability reasons. As expected, the flat Ni metalized samples, lacking any additional structures, showed the lowest catalytic activity of − 0.298 ± 0.010 V. This overpotential is rather high compared to reported values for high-performance Ni electrodes obtained via various other production techniques [2,25], but also comparable graphs histories can be found for Ni wires and powder [27] or films [24] showing higher overpotentials. For these samples, it should be considered that the surface roughness is very low meaning the surface area is small and $A_{geom}$ is equivalent to $A_{real}$. However, this simplifies the system and presents a sample perfectly suitable as baseline or reference for the conducted measurements. Also, the substrate is not conductive in this case, which can further influence the observed catalytic activity. The related influences of substrate choice and substrate requirements are not the focus of the present work and have been explained elsewhere [6,8,28–32]. Additionally, the standard deviation between the measured blank samples was found to be remarkably low, especially compared to other Ni catalysts in alkaline solutions [24,33,34]. This enhanced reproducibility is assigned to the careful and standardized production process, which was the initial aim of this work. Due to the effective surface increase, all structured samples are reproducibly more active than the blank reference. The structures of domes and cylinders exhibit comparable activities of − 0.264 ± 0.082 V and − 0.251 ± 0.042 V, while the star-structured electrodes exhibit slightly higher $\eta_{10\ geom}$ of − 0.277 ± 0.075 V. Due to the SEM analysis documenting the structural similarity between the dome and cylinder structures, also activities were expected to be in the same range. This trend was confirmed by the activity measurements. Notably, the star-structured electrodes have lower activities than the other surface geometries. This could be attributed to the lowest measured surface increase for the star structures. Whether the shift of the polarization curve and catalytic activity is purely guided by the surface increase is not distinguishable as presented. Therefore, also overpotentials for $A_{real}$ were calculated and added to Table T1. The compensation of the surface area for the structured electrodes leads to an alignment of the overpotential values $\eta_{10\ real}$ (see Fig. 5**(b)**). The recalculated activities per real surface area settle around the blank reference value. The compensation for the real surface area via the roughness factor confirms the dependence of the measured activity on the surface area. Within the limits of experimental accuracy, it is therefore concluded that in this experimental setup, the boost of catalytic activity is a mostly surface area-guided phenomenon in this experimental design. It has been documented elsewhere that the catalytic activity of Ni usually scales linearly with the surface area increase. However, the achievable highest activity is limited by the intrinsic catalytic activity of pure Ni [35]. To overcome this limitation, the introduction of further elements might be favorable either leading to Ni compounds (oxide, sulfide, phosphide) [25,35] or Ni-based alloys [2,36].

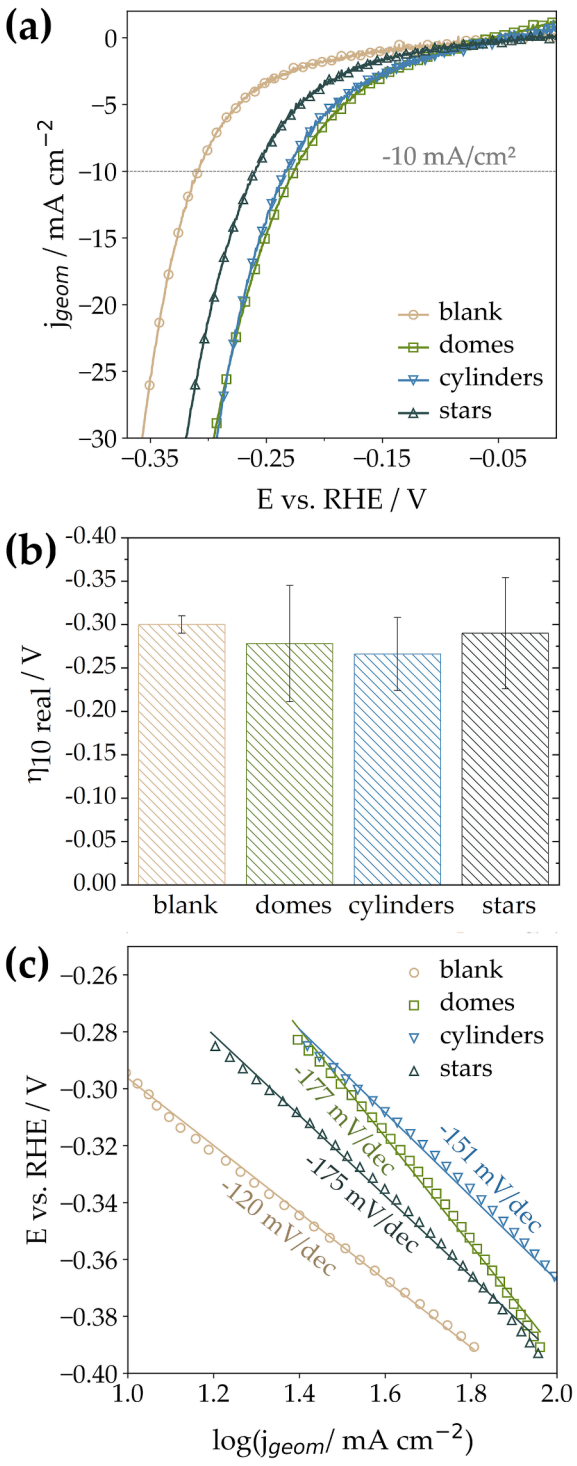


**Fig. 5.** Electrochemical evaluation of surface structures presenting (a) HER polarization curves of structured Ni thin film electrodes, (b) overpotentials (at −10 mA/cm$^2$) including standard deviation, after compensation for the effective electrode surface and (c) Tafel plots corresponding to the polarization curves.

Tafel analysis was performed on the polarization curves to obtain the Tafel slopes *b* shown in Fig. 5**(c)**. The Tafel slopes increase on structured surfaces compared to a flat electrode surface. A Tafel slope of −120 mV/dec was found for non-structured blank samples resembling a flat Ni

**Table T1**
Summary of Ni thin film electrode electrochemical data for (non-) structured samples, presented by the calculated roughness factors concerning the structured part only ($R_F$) and the effective electrode surface ($R_{F,eff.}$), the measured overpotentials at −10 mA cm$^{-2}$ based on the geometric ($\eta_{10\ geom}$) and the real ($\eta_{10\ real}$) surface area as well as corresponding Tafel slopes (b).

| Name | $R_F$ (structures) | $R_{F,\ eff.}$(electrode) | $\eta_{10\ geom}$ (V) | $\eta_{10\ real}$ (V) | *b* (mV dec$^{-1}$) |
|---|---|---|---|---|---|
| Blank | 1.02 ± 0.02 | 1.01 ± 0.08 | − (0.298 ± 0.010) | −(0.300 ± 0.010) | − (120 ± 11) |
| Domes | 1.60 | 1.25 | − (0.264 ± 0.082) | −(0.278 ± 0.067) | − (177 ± 17) |
| Cylinders | 1.60 | 1.25 | − (0.251 ± 0.042) | −(0.266 ± 0.042) | − (151 ± 9) |
| Stars | 1.60 | 1.25 | − (0.277 ± 0.075) | −(0.290 ± 0.064) | − (175 ± 46) |

electrode. This value is in excellent agreement with literature values for Ni electrodes [37,38]. A theoretical Tafel slope of −120 mV/dec can either be reached by a Volmer reaction-limited mechanism, or by a rate-limiting Heyrovsky reaction step with high hydrogen coverage [39]. In the chosen overpotential region, a high hydrogen coverage is expected and the Volmer-Heyrovsky reaction mechanism is suggested [38,40].

Ni electrodes are typically deactivated over time via hydride formation [33,41–43]. In the present work, we experienced a different limit of the electrodes due to the experimental design. The stability of the electrodes at this moment is limited to several cycles (supplementary **Fig. S7**). Finally, delamination of the Ni thin film will occur due to the non-optimized wet adhesion between the metallic thin film and the polymeric substrate. During catalyst application, an increase of $R_F$ on the flat Ni surface was noticed. This might occur due to periodic lattice changes and stresses occurring during the measurement cycles, which can subsequently promote surface roughening and delamination processes. For further optimization of the enrolled process, film wet adhesion, film stresses, and conductivity are to be addressed. In this study, the samples were closely checked for delamination after the measurements to ensure the reproducibility and reliability of the presented data. However, long-term observations (e.g. several hundred CV cycles) on the present specimen were prohibited due to an increasing tendency for delamination if experiments were extended over time.

As stated above, the electrocatalytic activity depends on the chosen substrate and can also be enhanced by substrate conductivity [44,45]. However, a basic preset for catalyst activity is also its inherent conductivity. In this work, polycrystalline metallic thin films were used, meaning the material conductivity itself should be sufficient. However, as depicted in Fig. 3, cracks appeared frequently on deposited thin films before and after use in the three-electrode setup. This could be problematic in terms of reproducibility if they are small or give rise to completely isolated regions. Moreover, the cracks potentially cause loss of conductivity and therefore disqualify those electrodes for further use due to severe connection problems. This issue can be attenuated by using conductive polymers as substrate to boost overall conductivity, lower electrode resistivity and compensate for potential minor thin film damage.

## 5. Discussion

The key advantages of the presented NIL approach based on MPL masks are structural versatility and fast manufacturing, rendering the approach ideal for structural investigations and fast iteration. However, the process should be briefly compared to masks and molds obtained by conventional UV or electron beam lithography [10,13,46–48]. Since no poisonous chemicals are involved in the MPL process, we consider this approach even more environmentally friendly compared to silicon etching, which still involves reactive fluorine ions or hydrofluoric acid etching [16,49]. Furthermore, the infrastructure required for MPL mask manufacturing is far less demanding compared to conventional lithographical mask writing. Despite these notable advantages, MPL mask writing suffers from one major drawback: the inferior resolution compared to silicon-based masks. The silicon mask approach enables feature sizes with defined edges at least one order of magnitude smaller [10,11,16]. Besides that, the mask materials are limited to the standard photopolymer, which might behave detrimentally upon multiple molding processes. For future mask writing, filled MPL resists, based on particles [50,51] or special monomers [52–55], will yield even more resilient masks, further narrowing the gap towards common glass or silicon masks from a material perspective.

With regards to shaping accuracy an implicit estimation can be carried out through information presented in **Fig. S2 and S4**. The "Tubes"-Structures exhibit only 80 % of the ideal diameter (see **Fig. S2**) and for a successful replica (see **Fig. S4**) 70 % of the ideal diameter is reached. The outer target dimension of all three investigated surface structures is about 3 μm, which yield roughly 2.7 μm after Ni deposition of 300 nm to each side, thus the final outer diameter should only deviate by roughly 10 %.

With this regard, the soft polymeric material used for deriving NIL molds, which is PDMS-based requires also a brief discussion. The PDMS initially selected due to the polymer's softness, thus facilitating the peel-off process from mask and replica, might not have been stable during successive replications in the used in combination with the UV-curable commercial photoresist. If monomers, solvents or other constituents of the liquid resist are absorbed into the PDMS swelling of the mold could be triggered, thus leading to loss of structural details on the replicas [56–58]. An actual shape change, later clarified and depicted in **Fig. S8**, might be related to this circumstance. With regards to the $R_f$ determined through CLSM a variation of surface factor by about 10 % could be identified. Although not used for the final evaluation, this might be related to the actual swelling of the PDMS mold and consequently a major contribution to the comparably large scattering in electrochemical data obtained.

However, this effect might be avoided in future works by choosing a more optimized molding material less prone to swelling. Besides that, no curing inhibition by any material pair, neither of the PDMS resin on the MPL photopolymer, nor of the commercial photoresist on the PDMS was observed. For alternative processes, the mold can be derived from any molding process, not harming the polymeric MPL-mask structures, including any other (finally soft) polymeric mold resin material curable via any mechanism. Even a very soft thermoplastic material should be suitable to imprint the MPL-structures if they are of low aspect ratio and not sheared off by friction due to the viscous flow. Deriving metallic molds directly from the master might be possible, but far more challenging with regards to separation since then both the MPL-substrate and mold material are stiff, which could require something like a soluble separation layer. Therefore, indirect methods might be required to obtain a metallic mold. A completely different approach could be the direct metallization of the PDMS (NIL mold structural as negative shape) through PVD, followed by a high-volume built-up process through e.g. electrodeposition to obtain a suitably stiff electrode base. Therefore, obtaining a fully metal electrode after peel-off, but constitutes a slower more complex process on the downside.

However, the NIL process in general shows promise in directly transferring the MPL shaping capability to a more efficient NIL process for rapid replication, rather than serving as a complete alternative to conventional mask production. The trend towards highly productive roll-process-based manufacturing of small-scale structures is gradually gaining attention [17–19,59]. Alternative methods for nano-structuring flexible ribbons have been proposed, which could be used as masks to create rolls or films suitable for continuous NIL replication. In this regard, in addition to a conventionally tiled mask for roll coating [47,60], Kronenfeld *et al.* [61] developed a roll-to-roll approach to facilitate continuous micro-3D printing onto a carrier foil. Also reversibly applied nanospheres were deposited onto a layer of photoresist through a roll-on-transfer, forming a self-assembled pattern acting as mask [49,62,63]. Although this approach has limited shaping possibilities, it demonstrates an unconventional and high-resolution approach for pattern application. Any of the outlined upscaling paths could find general application. Especially as most well-known surface structure effects, such as liquid and pollution-repelling lotus effect [64–66], imprinted optics [17,67], and bioactive surfaces [68], require a productive and reliable surface structuring technique for large-scale technical application. This holds also for upcoming technologies based on conductive polymers [69–72].

The method described here is especially suited for development. This makes it perfect for laboratory-scale research focusing on structure and material investigations, such as thin film catalyst electrodes. The actual results are shown in Fig. 5 and Table T1 and are briefly discussed in terms of their potential. The actual shape of the structure (cylinders vs. domes vs. stars) does not seem to influence the electrochemical parameters obtained through HER experiments, although strongly

deviating from the flat reference electrodes at first glance. After correcting for the surface area increase through structuring, the data of the structured electrodes aligns with the data of the reference electrode, if the scatter of the data is considered. Thus, no severe increase in catalytic activity due to the shape factor was observed reassembling the behavior of more or less flat Ni [24,27]. Consequently, the originally suggested increase in catalytic activity with regards to structure characteristics could not be confirmed, besides the overall increase in surface, and the various structure geometries must be seen as equivalently potent. The edges, originally considered sharp, did turn out considerably rounded (radius ~ 1 μm), and it is unclear if very sharp ones (down to ~ 100 nm) can be obtained this way. From the original MPL-structural precursors with a voxel diameter of < 400 nm, the NIL process replicates this radius in the best case, which is subsequently covered by 300 nm Ni, which additionally rounds the edges due to the deposition characteristic. Thus, the Ni film behaves quasi flat on a microstructural level. Defects within the film (pores, corners at the structure base, etc.) mediated by the structures' inherited roughness of the MPL-process seem not to cause any considerable effect.

Otherwise, the film thickness itself is a considerable factor with regards to catalytic activity [73–76]. The assessment and optimization of metal film thickness is not in the scope of this article, as there are too many additional factors to consider. Therefore, here only one specific aspect; the influence of surface structuring is considered and assessed with a direct comparison to unstructured (blank) electrode specimens.

However, surface structuring and structural refinement are well-known strategies to increase catalytic performance and reduce material loading. These strategies include surface decoration by nanostructures and the production of highly porous networks for surface area maximization. For example, templated grown 100 nm thick $TiO_2$ nanorods [63,77,78] and 100 nm thick ZnO nanowires [79] or tubes [3] decorated with Au nanoparticles enhance OER through photocatalysis. Equivalent improvements are known for HER catalysis [5,9]. Nanometer-sized dendrites [24] or micro/meso-porous foam [80] were found to perform intrinsically better in HER compared to a flat surface. This effect appears to be enhanced for nanoparticles with complex shapes, significantly improving their performance. [81]. Consequently, the surface structures selected herein might be too large to trigger an intrinsic effect via terraces, crystal orientation, or other mechanisms. This leaves the increase of effective surface area to be the most relevant factor in enhancing the performance. It should also be noted that fine structuring of printed polymer features, arising from surface discretization (line mismatch), could further influence the measured data. This is due to increased surface area and the potential creation of active low-coordination sites. The named structural features are most easily seen in the SEM image given for the dome structures in Fig. 4**(b)**. Huge potential in boosting the catalytic performance is seen in replacing the Ni thin film with an alloy [5]. Further enhancement could be achieved through suitable small-scale morphological structuring. $Ni/NiO_2$ nanoparticles on $CoSe_2$ nanobelts were found to show considerably higher HER catalysis (e.g. $\eta_{10}$ ~ -0.1 V) [82]. $Ni_2P$ nanoparticles could achieve a comparable result just without critical cobalt [83]. An HER activity even approaching that of gold standard platinum was obtained by a Ni foam electrode, exposing $MoNi_4$ and $MoO_2$ segregates on the surface [84]. For continuation and further investigations of the strategy developed in this work, the metallic thin film composition and the substrate material can be modified without actively altering one another. One improvement would be to subdivide the functionality of base coating and active HER sites to separate system layers. A crack-free and conductive film with enhanced wet adhesion properties could serve as base for nanoparticle decoration [81–84], forming catalytically active sites and boosting hydrogen evolution. Alternatively, the versatility of structuring allows diverse material processing paths starting from a polymeric base material. Thus, UV imprinting as performed in [85,86] might be carried out with a catalyst containing resin [87] or combined with polymerization-induced phase separation [88]. Hierarchical structures can be manufactured using an imprinting process [89,90], further enhancing the surface structure effect for HER [63,77–79].

## 6. Conclusion

In this study, a straightforward, dependable, and versatile method for surface structuring using MPL has been proposed. Exploring the possibilities of structure development yielded universal guidelines for structural design, suitable for the intended workflow proving the versatility of the process. Due to the structural replication via a well-known NIL replication with MPL-derived masks, an upscaling process is mimicked. This combination of steps makes the process suitable for manufacturing complex surface patterns, that can be used in a broad range of applications. As an inherently surface-sensitive application, the produced structures were tested in the context of HER catalysis. Therefore, the replicated structures were metalized and tested for their catalytic activity.

Upon further optimization within the limits of MPL resolution and material combination, even smaller feature sizes can be realized. Improvements regarding the mold material should be made to avoid swelling by the uptake of small molecules and therefore increase mold stability. This is equally true for the coating process, where the present case required a comparably thick Ni coating (of roughly 300 nm) to act as catalyst and ensure conductivity throughout the demanding experimental conditions. The surface area dependence of the catalytic performance was shown by studying structured thin film electrodes. However, a direct dependence of the activity on the structure shape was not found in this experimental design. Although a comparably simple structure design was utilized, more complex shapes can be straightforwardly manufactured through the spatial flexibility of MPL. Future designs might facilitate catalytic particle decoration or study hydrogen bubble-repelling structures or flow-directing facets which are important for electrode applications, but not directly related to the inherent catalytic activity.

It is concluded, that the structuring technique introduced in this work shows promise for industrial surface structuring applications, as it combines reliability, time efficiency and economic effectivity. Large-scale NIL molds through MPL-derived masks enable industrial process-driven development of combined functional surfaces.

## CRediT authorship contribution statement

**Alexander Jelinek:** Writing – original draft, Visualization, Methodology, Investigation, Formal analysis, Conceptualization. **Daniela Neumüller:** Writing – original draft, Visualization, Methodology, Investigation, Formal analysis, Conceptualization. **Christoph Gammer:** Writing – review & editing, Resources, Funding acquisition. **Jürgen Eckert:** Writing – review & editing. **Daniel Kiener:** Writing – review & editing, Resources, Funding acquisition.

## Declaration of competing interest

The authors declare that they have no known competing financial interests or personal relationships that could have appeared to influence the work reported in this paper.

## Acknowledgements

Daniela Nemüller and Alexander Jelinek contributed equally to this work. The infrastructure was funded by the Austrian Research Promotion Agency (FFG) in the framework of the F&E infrastructure program SmartNanoTop (ffg.at) [grant number 870449]. The authors acknowledge funding the European Research Council [grant number 771146] (DK) and partial funding by the OeAD GmbH [WTZ project number HR 07/2020]. The authors would like to thank Anna Hofer-Roblyek and Susanne Wenger from the Department of Materials Science at

Montanuniversität Leoben for conducting the micro scratch experiments.

## Appendix A. Supplementary data

Supplementary data to this article can be found online at https://doi.org/10.1016/j.matdes.2025.113809.

## Data availability

Data will be made available on request.

## References


[1] N.S. Hassan, A.A. Jalil, S. Rajendran, N.F. Khusnun, M.B. Bahari, A. Johari, M. J. Kamaruddin, M. Ismail, Recent review and evaluation of green hydrogen production via water electrolysis for a sustainable and clean energy society, Int. J. Hydrog. Energy 52 (2024) 420–441, https://doi.org/10.1016/j.ijhydene.2023.09.068.

[2] C.C.L. McCrory, S. Jung, I.M. Ferrer, S.M. Chatman, J.C. Peters, T.F. Jaramillo, Benchmarking hydrogen evolving reaction and oxygen evolving reaction electrocatalysts for solar water splitting devices, J. Am. Chem. Soc. 137 (2015) 4347–4357, https://doi.org/10.1021/ja510442p.

[3] M. Altomare, N.T. Nguyen, P. Schmuki, Templated dewetting: designing entirely self-organized platforms for photocatalysis, Chem. Sci. 7 (2016) 6865–6886, https://doi.org/10.1039/C6SC02555B.

[4] H. Lee, Utilization of shape-controlled nanoparticles as catalysts with enhanced activity and selectivity, RSC Adv. 4 (2014) 41017–41027, https://doi.org/10.1039/C4RA05958A.

[5] J. Zhu, L. Hu, P. Zhao, L.Y.S. Lee, K.-Y. Wong, Recent advances in electrocatalytic hydrogen evolution using nanoparticles, Chem. Rev. 120 (2020) 851–918, https://doi.org/10.1021/acs.chemrev.9b00248.

[6] I.A. Pašti, E. Fako, A.S. Dobrota, N. López, N.V. Skorodumova, S.V. Mentus, Atomically thin metal films on foreign substrates: from lattice mismatch to electrocatalytic activity, ACS Catal. 9 (2019) 3467–3481, https://doi.org/10.1021/acscatal.8b04236.

[7] J.H.J. Wijten, L.D.B. Mandemaker, T.C. Van Eeden, J.E. Dubbeld, B. M. Weckhuysen, In situ study on Ni–Mo stability in a water-splitting device: effect of catalyst substrate and electric potential, Chem. Sus. Chem. 13 (2020) 3172–3179, https://doi.org/10.1002/cssc.202000678.

[8] H. Wei, J. Liu, Y. Deng, W. Hu, C. Zhong, Studies on the effect of the substrate on the electrocatalytic performance of electrodeposited NiFe hydroxides for oxygen evolution reaction, Int. J. Electochem. Sci. 14 (2019) 4173–4184, https://doi.org/10.20964/2019.05.45.

[9] Z.W. Seh, J. Kibsgaard, C.F. Dickens, I. Chorkendorff, J.K. Nørskov, T.F. Jaramillo, Combining theory and experiment in electrocatalysis: Insights into materials design, eaad4998, Science 355 (2017), https://doi.org/10.1126/science:aad4998.

[10] L.J. Guo, Nanoimprint lithography: methods and material requirements, Adv. Mater. 19 (2007) 495–513, https://doi.org/10.1002/adma.200600882.

[11] S.V. Sreenivasan, Nanoimprint lithography steppers for volume fabrication of leading-edge semiconductor integrated circuits, Microsyst. Nanoeng. 3 (2017) 17075, https://doi.org/10.1038/micronano.2017.75.

[12] H. Schift, Nanoimprint lithography: An old story in modern times? A review, J. Vac. Sci. Technol. B 26 (2008) 458–480, https://doi.org/10.1116/1.2890972.

[13] A. Hager, L. Güniat, N. Morgan, S.P. Ramanandan, A. Rudra, V. Piazza, A. Fontcuberta I Morral, D. Dede, The implementation of thermal and UV nanoimprint lithography for selective area epitaxy, Nanotechnol. 34 (2023) 445301. 10.1088/1361-6528/acea87.

[14] L.M. Cox, A.M. Martinez, A.K. Blevins, N. Sowan, Y. Ding, C.N. Bowman, Nanoimprint lithography: Emergent materials and methods of actuation, Nano Today 31 (2020) 100838, https://doi.org/10.1016/j.nantod.2019.100838.

[15] B. Sölle, D. Reisinger, S. Heupl, A. Jelinek, S. Schlögl, E. Rossegger, Reshapable bio-based thiol-ene vitrimers for nanoimprint lithography: Advanced covalent adaptability for tunable surface properties, React. Funct. Polym. 202 (2024) 105972, https://doi.org/10.1016/j.reactfunctpolym.2024.105972.

[16] Y. Chen, Applications of nanoimprint lithography/hot embossing: a review, Appl. Phys. A 121 (2015) 451–465, https://doi.org/10.1007/s00339-015-9071-x.

[17] K. Nagato, K. Takahashi, Y. Yajima, M. Nakao, Laser-assisted direct roller imprinting of large-area microstructured optical surfaces, Microsyst. Nanoeng. 10 (2024) 9, https://doi.org/10.1038/s41378-024-00650-3.

[18] J.G. Ok, M.K. Kwak, C.M. Huard, H.S. Youn, L.J. Guo, Photo–Roll Lithography (PRL) for continuous and scalable patterning with application in flexible electronics, Adv. Mater. 25 (2013) 6554–6561, https://doi.org/10.1002/adma.201303514.

[19] H.J. Park, M. Kang, S.H. Ahn, L.J. Guo, A facile route to polymer solar cells with optimum morphology readily applicable to a roll-to-roll process without sacrificing high device performances, Adv. Mater. 22 (2010) E247–E253, https://doi.org/10.1002/adma.201000250.

[20] D. Yu, D. Beckelmann, M. Opsölder, B. Schäfer, K. Moh, R. Hensel, P.W. De Oliveira, E. Arzt, Roll-to-roll manufacturing of micropatterned adhesives by template compression, Materials 12 (2018) 97, https://doi.org/10.3390/ma12010097.

[21] A. Jelinek, S. Zak, M. Alfreider, D. Kiener, High-throughput micromechanical testing enabled by optimized direct laser writing, Adv. Eng. Mater. (2022) 2200288, https://doi.org/10.1002/adem.202200288.

[22] M.H. Miles, M.A. Thomason, Periodic variations of overvoltages for water electrolysis in acid solutions from cyclic voltammetric studies, J. Electrochem. Soc. 123 (1976) 1459–1461, https://doi.org/10.1149/1.2132619.

[23] C. Wang, Z. Wang, S. Mao, Z. Chen, Y. Wang, Coordination environment of active sites and their effect on catalytic performance of heterogeneous catalysts, Chin. J. Catal. 43 (2022) 928–955, https://doi.org/10.1016/S1872-2067(21)63924-4.

[24] S.H. Ahn, S.J. Hwang, S.J. Yoo, I. Choi, H.-J. Kim, J.H. Jang, S.W. Nam, T.-H. Lim, T. Lim, S.-K. Kim, J.J. Kim, Electrodeposited Ni dendrites with high activity and durability for hydrogen evolution reaction in alkaline water electrolysis, J. Mater. Chem. 22 (2012) 15153, https://doi.org/10.1039/c2jm31439h.

[25] D. Neumüller, L.D. Rafailović, A.Z. Jovanović, N.V. Skorodumova, I.A. Pašti, A. Lassnig, T. Griesser, C. Gammer, J. Eckert, Hydrogen evolution reaction on ultra-smooth sputtered nanocrystalline Ni thin films in alkaline media—from intrinsic activity to the effects of surface oxidation, Nanomaterials 13 (2023) 2085, https://doi.org/10.3390/nano13142085.

[26] D. Nečas, P. Klapetek, Gwyddion: an open-source software for SPM data analysis, Open Phys. 10 (2012) 181–188, https://doi.org/10.2478/s11534-011-0096-2.

[27] J.R. McKone, B.F. Sadtler, C.A. Werlang, N.S. Lewis, H.B. Gray, Ni–Mo nanopowders for efficient electrochemical hydrogen evolution, ACS Catal. 3 (2013) 166–169, https://doi.org/10.1021/cs300691m.

[28] A. Schlapka, M. Lischka, A. Groß, U. Käsberger, P. Jakob, Surface strain versus substrate interaction in heteroepitaxial metal layers: Pt on Ru(0001), Phys. Rev. Lett. 91 (2003) 016101, https://doi.org/10.1103/PhysRevLett.91.016101.

[29] M. Mavrikakis, B. Hammer, J.K. Nørskov, Effect of strain on the reactivity of metal surfaces, Phys. Rev. Lett. 81 (1998) 2819–2822, https://doi.org/10.1103/PhysRevLett.81.2819.

[30] H. Wang, S. Xu, C. Tsai, Y. Li, C. Liu, J. Zhao, Y. Liu, H. Yuan, F. Abild-Pedersen, F. B. Prinz, J.K. Nørskov, Y. Cui, Direct and continuous strain control of catalysts with tunable battery electrode materials, Science 354 (2016) 1031–1036, https://doi.org/10.1126/science:aaf7680.

[31] M. Gsell, P. Jakob, D. Menzel, Effect of substrate strain on adsorption, Science 280 (1998) 717–720, https://doi.org/10.1126/science:280.5364.717.

[32] J. Som, J. Choi, H. Zhang, N. Reddy Mucha, S. Fialkova, K. Mensah-Darkwa, J. Suntivich, R.K. Gupta, D. Kumar, Effect of substrate-induced lattice strain on the electrochemical properties of pulsed laser deposited nickel oxide thin film, Mater. Sci. Eng. B 280 (2022) 115711, https://doi.org/10.1016/j.mseb.2022.115711.

[33] D.S. Hall, C. Bock, B.R. MacDougall, The electrochemistry of metallic nickel: oxides, hydroxides, hydrides and alkaline hydrogen evolution, J. Electrochem. Soc. 160 (2013) F235–F243, https://doi.org/10.1149/2.026303jes.

[34] A. Lasia, Hydrogen evolution reaction, in: W. Vielstich, A. Lamm, H.A. Gasteiger, H. Yokokawa (Eds.), Handbook of Fuel Cells, 1st ed.,, Wiley, 2010, https://doi.org/10.1002/9780470974001.f204033.

[35] M. Gong, D.-Y. Wang, C.-C. Chen, B.-J. Hwang, H. Dai, A mini review on nickel-based electrocatalysts for alkaline hydrogen evolution reaction, Nano Res. 9 (2016) 28–46, https://doi.org/10.1007/s12274-015-0965-x.

[36] D. Neumüller, L.D. Rafailović, I.A. Pašti, T. Griesser, C. Gammer, J. Eckert, Revealing the role of Mo leaching in the structural transformation of NiMo thin film catalysts upon hydrogen evolution reaction, Small (2024) 2402200, https://doi.org/10.1002/smll.202402200.

[37] M. Grdeń, G. Jerkiewicz, Influence of surface treatment on the kinetics of the hydrogen evolution reaction on bulk and porous nickel materials, Electrocatalysis 10 (2019) 173–183, https://doi.org/10.1007/s12678-019-0506-6.

[38] N. Krstajic, M. Popovic, B. Grgur, M. Vojnovic, On the kinetics of the hydrogen evolution reaction on nickel in alkaline solution Part I. The mechanism, J. Electroanal. Chem. 512 (2001) 16–26.

[39] T. Shinagawa, A.T. Garcia-Esparza, K. Takanabe, Insight on Tafel slopes from a microkinetic analysis of aqueous electrocatalysis for energy conversion, Sci. Rep. 5 (2015) 13801, https://doi.org/10.1038/srep13801.

[40] A. Lasia, A. Rami, Kinetics of hydrogen evolution on nickel electrodes, J. Electroanal. Chem. 294 (1990) 123–141, https://doi.org/10.1016/0022-0728(90)87140-F.

[41] R.M. Abouatallah, D.W. Kirk, J.W. Graydon, Long-term electrolytic hydrogen permeation in nickel and the effect of vanadium species addition, Electrochim. Acta 47 (2002) 2483–2494, https://doi.org/10.1016/S0013-4686(02)00108-1.

[42] H.E.G. Rommal, P.J. Morgan, The role of absorbed hydrogen on the voltage-time behavior of nickel cathodes in hydrogen evolution, J. Electrochem. Soc. 135 (1988) 343–346, https://doi.org/10.1149/1.2095612.

[43] D.M. Soares, O. Teschke, I. Torriani, Hydride effect on the kinetics of the hydrogen evolution reaction on nickel cathodes in alkaline media, J. Electrochem. Soc. 139 (1992) 98–105, https://doi.org/10.1149/1.2069207.

[44] K. Namsheer, C.S. Rout, Conducting polymers: a comprehensive review on recent advances in synthesis, properties and applications, RSC Adv. 11 (2021) 5659–5697, https://doi.org/10.1039/D0RA07800J.

[45] B. Hüner, N. Demir, M.F. Kaya, Electrodeposition of NiCu bimetal on 3D printed electrodes for hydrogen evolution reactions in alkaline media, Int. J. Hydrog. Energy 47 (2022) 12136–12146, https://doi.org/10.1016/j.ijhydene.2021.10.009.

[46] P. Bhagoria, E. Mathew Sebastian, S. Kumar Jain, J. Purohit, R. Purohit, Nanolithography and its alternate techniques, Mater. Today: Proc. 26 (2020) 3048–3053, https://doi.org/10.1016/j.matpr.2020.02.633.

[47] C.H. Moon, K.-S. Han, M. Kim, D.K. Oh, S. Yi, T. Kim, H. Kim, J. Hwang, J.G. Nam, D.-E. Lee, D.-Y. Lee, G.R. Jo, J.G. Ok, Scaling up the sub-50 nm-resolution roll-to-roll nanoimprint lithography process via large-area tiling of flexible molds and

uniform linear UV curing, J. Mech. Sci. Technol. 37 (2023) 271–278, https://doi.org/10.1007/s12206-022-1227-y.
[48] B. Radha, S.H. Lim, M.S.M. Saifullah, G.U. Kulkarni, Metal hierarchical patterning by direct nanoimprint lithography, Sci. Rep. 3 (2013) 1078, https://doi.org/10.1038/srep01078.
[49] M. Fang, H. Lin, H.-Y. Cheung, F. Xiu, L. Shen, S. Yip, E.-Y.-B. Pun, C.-Y. Wong, J. C. Ho, Polymer-confined colloidal monolayer: a reusable soft photomask for rapid wafer-scale nanopatterning, ACS Appl. Mater. Interf. 6 (2014) 20837–20841, https://doi.org/10.1021/am505221g.
[50] F. Kotz, A.S. Quick, P. Risch, T. Martin, T. Hoose, M. Thiel, D. Helmer, B.E. Rapp, Two-photon polymerization of nanocomposites for the fabrication of transparent fused silica glass microstructures, Adv. Mater. 33 (2021) 2006341, https://doi.org/10.1002/adma.202006341.
[51] J.C. Sänger, B.R. Pauw, H. Sturm, J. Günster, First time additively manufactured advanced ceramics by using two-photon polymerization for powder processing, Open Ceram. 4 (2020) 100040, https://doi.org/10.1016/j.oceram.2020.100040.
[52] A. Doraiswamy, C. Jin, R. Narayan, P. Mageswaran, P. Mente, R. Modi, R. Auyeung, D. Chrisey, A. Ovsianikov, B. Chichkov, Two photon induced polymerization of organic–inorganic hybrid biomaterials for microstructured medical devices, Acta Biomater. 2 (2006) 267–275, https://doi.org/10.1016/j.actbio.2006.01.004.
[53] A. Vyatskikh, S. Delalande, A. Kudo, X. Zhang, C.M. Portela, J.R. Greer, Additive manufacturing of 3D nano-architected metals, Nat. Commun. 9 (2018) 593, https://doi.org/10.1038/s41467-018-03071-9.
[54] E. Balčiūnas, S.J. Baldock, N. Dreižė, M. Grubliauskaitė, S. Coultas, D.L. Rochester, M. Valius, J.G. Hardy, D. Baltriukienė, 3D printing hybrid organometallic polymer-based biomaterials via laser two-photon polymerization, Poly. Int. 68 (2019) 1928–1940, https://doi.org/10.1002/pi.5909.
[55] Z. Faraji Rad, P.D. Prewett, G.J. Davies, High-resolution two-photon polymerization: the most versatile technique for the fabrication of microneedle arrays, Microsyst. Nanoeng. 7 (2021) 71, https://doi.org/10.1038/s41378-021-00298-3.
[56] I.W. Moran, A.L. Briseno, S. Loser, K.R. Carter, Device fabrication by easy soft imprint nano-lithography, Chem. Mater. 20 (2008) 4595–4601, https://doi.org/10.1021/cm800480z.
[57] K.W. Bong, J. Xu, J.-H. Kim, S.C. Chapin, M.S. Strano, K.K. Gleason, P.S. Doyle, Non-polydimethylsiloxane devices for oxygen-free flow lithography, Nat. Commun. 3 (2012) 805, https://doi.org/10.1038/ncomms1800.
[58] J.J. Dumond, H.Y. Low, H.P. Lee, J.Y.H. Fuh, Multi-functional silicone stamps for reactive release agent transfer in UV roll-to-roll nanoimprinting, Mater. Horiz. 3 (2016) 152–160, https://doi.org/10.1039/C5MH00290G.
[59] J. Kim, N. Krishna-Subbaiah, Y. Wu, J. Ko, A. Shiva, M. Sitti, Enhanced flexible mold lifetime for roll-to-roll scaled-up manufacturing of adhesive complex microstructures, Adv. Mater. 35 (2023) 2207257, https://doi.org/10.1002/adma.202207257.
[60] S. Koo, S.H. Lee, J.D. Kim, J.G. Hong, H.W. Baac, M.K. Kwak, J.G. Ok, Controlled airbrush coating of polymer resists in Roll-to-Roll nanoimprinting with regimented residual layer thickness, Int. J. Precis. Eng. Manuf. 17 (2016) 943–947, https://doi.org/10.1007/s12541-016-0115-8.
[61] J.M. Kronenfeld, L. Rother, M.A. Saccone, M.T. Dulay, J.M. DeSimone, Roll-to-roll, high-resolution 3D printing of shape-specific particles, Nature 627 (2024) 306–312, https://doi.org/10.1038/s41586-024-07061-4.
[62] I.-T. Chen, E. Schappell, X. Zhang, C.-H. Chang, Continuous roll-to-roll patterning of three-dimensional periodic nanostructures, Microsyst. Nanoeng. 6 (2020) 22, https://doi.org/10.1038/s41378-020-0133-7.
[63] W. Wang, J. Dong, X. Ye, Y. Li, Y. Ma, L. Qi, Heterostructured TiO $_2$ nanorod@nanobowl arrays for efficient photoelectrochemical water splitting, Small 12 (2016) 1469–1478, https://doi.org/10.1002/smll.201503553.
[64] H.-X. Huang, X. Wang, Biomimetic fabrication of micro-/nanostructure on polypropylene surfaces with high dynamic superhydrophobic stability, Mater. Today Commun. 19 (2019) 487–494, https://doi.org/10.1016/j.mtcomm.2019.04.005.
[65] M. Muehlberger, Nanoimprinting of biomimetic nanostructures, Nanomanuf. 2 (2022) 17–40, https://doi.org/10.3390/nanomanufacturing2010002.
[66] J.J. Hernández, M.A. Monclús, I. Navarro-Baena, F. Viela, J.M. Molina-Aldareguia, I. Rodríguez, Multifunctional nano-engineered polymer surfaces with enhanced mechanical resistance and superhydrophobicity, Sci. Rep. 7 (2017) 43450, https://doi.org/10.1038/srep43450.
[67] L. Kuna, C. Leiner, W. Nemitz, F. Reil, P. Hartmann, F.-P. Wenzl, C. Sommer, Optical design of freeform micro-optical elements and their fabrication combining maskless laser direct write lithography and replication by imprinting, J. Photon. Energy 7 (2017) 016002, https://doi.org/10.1117/1.JPE.7.016002.
[68] F. Cai, A. Blanquer, M.B. Costa, L. Schweiger, B. Sarac, A.L. Greer, J. Schroers, C. Teichert, C. Nogués, F. Spieckermann, J. Eckert, Hierarchical surface pattern on Ni-free Ti-based bulk metallic glass to control cell interactions, Small 20 (2024) 2310364, https://doi.org/10.1002/smll.202310364.
[69] B. Oh, S. Baek, K.S. Nam, C. Sung, C. Yang, Y.-S. Lim, M.S. Ju, S. Kim, T.-S. Kim, S.-M. Park, S. Park, S. Park, 3D printable and biocompatible PEDOT:PSS-ionic liquid colloids with high conductivity for rapid on-demand fabrication of 3D bioelectronics, Nat. Commun. 15 (2024) 5839, https://doi.org/10.1038/s41467-024-50264-6.
[70] J. Byun, B. Lee, E. Oh, H. Kim, S. Kim, S. Lee, Y. Hong, Fully printable, strain-engineered electronic wrap for customizable soft electronics, Sci. Rep. 7 (2017) 45328, https://doi.org/10.1038/srep45328.
[71] S. Jeong, H. Yoon, L.F. Michalek, G. Kim, J. Kim, J. Seo, D. Kim, H. Park, B. Lee, Y. Hong, Printable, stretchable metal-vapor-desorption layers for high-fidelity patterning in soft, freeform electronics, Nat. Commun. 15 (2024) 7209, https://doi.org/10.1038/s41467-024-51585-2.
[72] U. Palfinger, C. Auner, H. Gold, A. Haase, J. Kraxner, T. Haber, M. Sezen, W. Grogger, G. Domann, G. Jakopic, J.R. Krenn, B. Stadlober, Fabrication of n- and p-type organic thin film transistors with minimized gate overlaps by self-aligned nanoimprinting, Adv. Mater. 22 (2010) 5115–5119, https://doi.org/10.1002/adma.201001947.
[73] M. Kozejova, R. Bodnarova, V. Latyshev, M. Lisnichuk, V. Girman, H. You, V. Komanicky, Structural dependence of hydrogen evolution reaction on transition metal catalysts sputtered at different temperatures in alkaline media, Int. J. Hydrog. Energy 47 (2022) 26987–26999, https://doi.org/10.1016/j.ijhydene.2022.06.036.
[74] K. Sahu, A. Bisht, S.A. Khan, I. Sulania, R. Singhal, A. Pandey, S. Mohapatra, Thickness dependent optical, structural, morphological, photocatalytic and catalytic properties of radio frequency magnetron sputtered nanostructured Cu2O–CuO thin films, Ceram. Int. 46 (2020) 14902–14912, https://doi.org/10.1016/j.ceramint.2020.03.017.
[75] L.A. Kibler, Dependence of electrocatalytic activity on film thickness for the hydrogen evolution reaction of Pd overlayers on Au(111), Electrochim. Acta 53 (2008) 6824–6828, https://doi.org/10.1016/j.electacta.2008.01.097.
[76] R.K. Patel, R.N. Jenjeti, R. Kumar, N. Bhattacharya, S. Kumar, S.K. Ojha, Z. Zhang, H. Zhou, K. Qu, Z. Wang, Z. Yang, C. Klewe, P. Shafer, S. Sampath, S. Middey, Thickness dependent OER electrocatalysis of epitaxial thin film of high entropy oxide, Appl. Phys. Rev. 10 (2023) 031407, https://doi.org/10.1063/5.0146005.
[77] Z. Xu, M. Yin, J. Sun, G. Ding, L. Lu, P. Chang, X. Chen, D. Li, 3D periodic multiscale TiO $_2$ architecture: a platform decorated with graphene quantum dots for enhanced photoelectrochemical water splitting, Nanotechnol. 27 (2016) 115401, https://doi.org/10.1088/0957-4484/27/11/115401.
[78] M. Fang, G. Dong, R. Wei, J.C. Ho, Hierarchical nanostructures: design for sustainable water splitting, Adv. Energy Mat. 7 (2017) 1700559, https://doi.org/10.1002/aenm.201700559.
[79] P. Thiyagarajan, H. Ahn, J. Lee, J. Yoon, J. Jang, Hierarchical metal/semiconductor nanostructure for efficient water splitting, Small 9 (2013) 2341–2347, https://doi.org/10.1002/smll.201202756.
[80] T. Sun, C. Zhang, J. Chen, Y. Yan, A.A. Zakhidov, R.H. Baughman, L. Xu, Three-dimensionally ordered macro-/mesoporous Ni as a highly efficient electrocatalyst for the hydrogen evolution reaction, J. Mater. Chem. A 3 (2015) 11367–11375, https://doi.org/10.1039/C5TA01383F.
[81] S.A. Abbas, M.I. Iqbal, S.-H. Kim, K.-D. Jung, Catalytic activity of urchin-like ni nanoparticles prepared by solvothermal method for hydrogen evolution reaction in alkaline solution, Electrochim. Acta 227 (2017) 382–390, https://doi.org/10.1016/j.electacta.2017.01.039.
[82] Y. Xu, M. Gao, Y. Zheng, J. Jiang, S. Yu, Nickel/nickel(II) oxide nanoparticles anchored onto cobalt(IV) diselenide nanobelts for the electrochemical production of hydrogen, Angew. Chem. Int. Ed. 52 (2013) 8546–8550, https://doi.org/10.1002/anie.201303495.
[83] E.J. Popczun, J.R. McKone, C.G. Read, A.J. Biacchi, A.M. Wiltrout, N.S. Lewis, R. E. Schaak, Nanostructured nickel phosphide as an electrocatalyst for the hydrogen evolution reaction, J. Am. Chem. Soc. 135 (2013) 9267–9270, https://doi.org/10.1021/ja403440e.
[84] J. Zhang, T. Wang, P. Liu, Z. Liao, S. Liu, X. Zhuang, M. Chen, E. Zschech, X. Feng, Efficient hydrogen production on MoNi4 electrocatalysts with fast water dissociation kinetics, Nat. Commun. 8 (2017) 15437, https://doi.org/10.1038/ncomms15437.
[85] C.-Y. Yang, M.-A. Stoeckel, T.-P. Ruoko, H.-Y. Wu, X. Liu, N.B. Kolhe, Z. Wu, Y. Puttisong, C. Musumeci, M. Massetti, H. Sun, K. Xu, D. Tu, W.M. Chen, H. Y. Woo, M. Fahlman, S.A. Jenekhe, M. Berggren, S. Fabiano, A high-conductivity n-type polymeric ink for printed electronics, Nat. Commun. 12 (2021) 2354, https://doi.org/10.1038/s41467-021-22528-y.
[86] Y. Kim, C. Park, S. Im, J.H. Kim, Design of intrinsically stretchable and highly conductive polymers for fully stretchable electrochromic devices, Sci. Rep. 10 (2020) 16488, https://doi.org/10.1038/s41598-020-73259-x.
[87] X. He, B. Zhang, Q. Liu, H. Chen, J. Cheng, B. Jian, H. Yin, H. Li, K. Duan, J. Zhang, Q. Ge, Highly conductive and stretchable nanostructured ionogels for 3D printing capacitive sensors with superior performance, Nat. Commun. 15 (2024) 6431, https://doi.org/10.1038/s41467-024-50797-w.
[88] B. Deore, K.L. Sampson, T. Lacelle, N. Kredentser, J. Lefebvre, L.S. Young, J. Hyland, R.E. Amaya, J. Tanha, P.R.L. Malenfant, H.W. De Haan, C. Paquet, Direct printing of functional 3D objects using polymerization-induced phase separation, Nat. Commun. 12 (2021) 55, https://doi.org/10.1038/s41467-020-20256-3.
[89] H. Cho, J. Kim, H. Park, J. Won Bang, M. Seop Hyun, Y. Bae, L. Ha, D. Yoon Kim, S. Min Kang, T. Jung Park, S. Seo, M. Choi, K.-Y. Suh, Replication of flexible polymer membranes with geometry-controllable nano-apertures via a hierarchical mould-based dewetting, Nat. Commun. 5 (2014) 3137, https://doi.org/10.1038/ncomms4137.
[90] A.R. Moharana, H.M. Außerhuber, T. Mitteramskogler, M.J. Haslinger, M. M. Mühlberger, Multilayer nanoimprinting to create hierarchical stamp masters for nanoimprinting of optical micro- and nanostructures, Coatings 10 (2020) 301, https://doi.org/10.3390/coatings10030301.